Appl. Phys. B 85, 397–406 (2006)
DOI: 10.1007/s00340-006-2356-1

Applied Physics B
Lasers and Optics

E.R.T. KERSTEL[1,✉]
R.Q. IANNONE[1]
M. CHENEVIER[2]
S. KASSI[2]
H.-J. JOST[3,*]
D. ROMANINI[2]

A water isotope (^{2}H, ^{17}O, and ^{18}O) spectrometer based on optical feedback cavity-enhanced absorption for in situ airborne applications

[1] Department of Physics, Center for Isotope Research, University of Groningen, 9747 AG Groningen, The Netherlands
[2] Laboratoire de Spectrométrie Physique, CNRS UMR5588, Université Joseph Fourier Grenoble, Saint Martin d'Hères, France
[3] Bay Area Environmental Research Institute, Sonoma, CA 95476, USA

Received: 2 May 2006/Revised version: 29 May 2006
Published online: 25 July 2006 •

ABSTRACT Measurements of the isotopic composition of water are thought to help explain stratospheric aridity and related issues in atmospheric sciences. Simultaneous in situ measurements of ^{2}H/^{1}H, ^{17}O/^{16}O, and ^{18}O/^{16}O at high spatial resolution are required for this purpose. We present the design and laboratory performance of a device that will be used on high-altitude research aircraft. It is based on optical feedback cavity-enhanced spectroscopy (OF-CEAS), with better sensitivity than traditional multi-pass arrangements. It utilizes a near-infrared laser source, avoiding the need for cryogens. We demonstrate an airborne precision during tropospheric flight conditions of 1‰, 3‰, and 9‰ for δ^{18}O, δ^{17}O, and δ^2H, respectively, for 30-s averaged data and a water concentration of about 200 ppm. With recent improvements we expect to remain within a factor of about three of these values under true stratospheric conditions (water mixing ratio ∼ 10 ppmv).

PACS 07.88.+y; 42.55.Px; 42.62.Fi; 92.60.Hd; 92.60.Jq

1 Introduction

Water is arguably the most important molecule in the Earth's atmosphere. The large enthalpy change associated with the evaporation and condensation of water causes it to dominate the global redistribution of energy by tropospheric transport of latent heat. Water vapor is also the most important greenhouse gas. In the stratosphere, water vapor affects both radiative forcing and chemistry [1, 2]. Through its reaction with excited oxygen ^{1}D atoms, stratospheric water is the major source of hydroxyl radicals, controlling the oxidative capacity of the atmosphere, including ozone chemistry and methane oxidation [3, 4]. In addition, water vapor is an important constituent of polar stratospheric clouds, which modulate polar ozone destruction.

Despite its importance for the climate and our ability to predict future climate change, our understanding of the water cycle and transport into the stratosphere is still very limited. Remote sensing and in situ measurements indicate a trend of increasing water concentrations in the stratosphere in recent decades, from roughly 4 ppm in the 1950s to about 6 ppm today [5, 6]. Recently, it has been noted that this trend may have reversed in satellite data [7]. Reasons for these important changes are still poorly understood. About one-half of the observed increase may be attributed to an anthropogenic increase of the methane concentration [6], while the remainder could be caused by direct injection into the stratosphere [8] or by an enhanced methane oxidation efficiency due to an increase in anthropogenic chlorine [9, 10].

Understanding the process of dehydration of air entering the stratosphere through the tropical tropopause, and the origin and microphysical properties of radiatively important thin cirrus clouds in the tropical tropopause, are among the key problems in atmospheric science.

There are currently two competing hypotheses that attempt to explain the extreme aridity of the stratosphere. Both agree that the main entry point for water vapor is in the tropics and that instead of thinking of the tropopause as an infinitely thin layer, the troposphere and stratosphere should be thought of as being separated by a layer several kilometers thick. Sherwood and Dessler defined this tropical tropopause layer (TTL) as extending from 12 to 19 km [11]. Whereas air arriving at the bottom of the TTL still contains several tens of ppmv of water vapor and condensate, the air passing into the stratosphere contains on average less than 4 ppmv water. Sherwood and Dessler proposed that convection lifts the air to above its level of neutral buoyancy, normally near the bottom of the TTL, where it experiences temperatures sufficiently low that the air emerges with stratospheric humidity levels [12, 13]. This hypothesis may be termed 'convective (overshooting) dehydration'. The competing hypothesis was suggested by Holton and Gettelman [14] and Jensen et al. [15] and is known as 'gradual dehydration'. In this case, air still relatively moist detrains from convection near its level of natural buoyancy. While slowly ascending, the air mass makes large-scale quasi-horizontal motions through regions where the cold-point temperatures are anomalously low, such as the 'cold trap' of the western Pacific. This then leads to the formation and subsequent sedimentation of particles that dehydrate the air. Since their introduction, both models have been further refined and adapted, but the central premises remain intact. Both are able to accurately reproduce many observa-

✉ Fax: +31-50-363 4738, E-mail: e.r.t.kerstel@rug.nl
Now at: NovaWave Technologies, Redwood City, CA 94065, USA

tional water-distribution data, but differ in their predictions of the behavior of the different isotopologues, especially their vertical profiles [11].

Measurements of the isotopic composition of water vapor in the upper troposphere and lower stratosphere are therefore vital in testing the various hypotheses of stratospheric aridity. This is mainly due to changes in isotopic composition that accompany phase changes and chemical reactions as a result of the usually higher binding energy of the heavier isotopologues and their lower mobility, which in turn lead to a lower vapor pressure and a lower reactivity. Thus, in the tropospheric hydrological cycle, water vapor becomes gradually depleted in the heavier isotopologues as seawater evaporates (predominantly in the tropics), and the generated moisture then preferentially loses the heavier isotopologues in condensation events during the transport to higher altitudes and higher latitudes. Water vapor entering the tropopause region typically contains about 650 ‰ (i.e. 65%) less ^{2}H and about 100 ‰ less ^{18}O than ocean water.

By convention, the isotope abundances are expressed in terms of the so-called 'δ value': the relative deviation of the rare to abundant isotope ratio in a sample with respect to the same ratio in a reference material. For example, in the case of deuterium,

$$\delta^2\mathrm{H} = \frac{{}^2R_{\mathrm{sample}}}{{}^2R_{\mathrm{reference}}} - 1\,, \tag{1}$$

where ${}^2R$ represents the ratio of rare to abundant isotopes. Since the changes in the δ values are small, it is customary to express the value in per mil. One can show that the atomic δ value (${}^2R = [\mathrm{D}]/[\mathrm{H}]$) is in all practical situations equal to the molecular δ value (${}^2R = [\mathrm{HOD}]/(2[\mathrm{H_2O}])$, where the factor of two accounts for the two equivalent positions of the hydrogen atom in the water molecule [16]. The internationally accepted reference material for water is known as Vienna Standard Mean Ocean Water (VSMOW). In general one would use a laboratory secondary standard for actual measurements that, however, can be traced back to VSMOW by repeated mass-spectrometry analyses.

According to the Tropical Composition, Cloud and Climate Coupling Experiment (TC4) white paper [17] the following five (out of eight listed) science questions can be addressed by water isotope ratio measurements:

1. What mechanisms maintain the humidity of the stratosphere? What are the relative roles of large-scale transport and convective transport and how are these processes coupled?
2. What are the physical mechanisms that control (and cause) long-term changes in the humidity of the upper troposphere in the tropics and subtropics?
3. What controls the formation and distribution of thin cirrus in the TTL, and what is the influence of thin cirrus on radiative heating and cooling rates, and on vertical transport?
4. How do convective intensity and aerosol properties affect cirrus anvil properties?
5. How do cirrus anvils, and tropical cirrus in general, evolve over their life cycle? How do they impact the radiation budget and ultimately the circulation?

Another interesting issue that can be addressed by isotope measurements is the extent to which the ^{17}O anomaly observed in ozone is transferred to water. Whereas all tropospheric water exhibits a strong correlation between δ^{17}O and δ^{18}O of the form $(1+\delta^{17}\mathrm{O}) = (1+\delta^{18}\mathrm{O})^{0.528}$ [18], referred to as mass-dependent fractionation, this may no longer be true for stratospheric water due to oxygen-exchange reactions between HO_x and NO_x, $\mathrm{O}(^1\mathrm{D})$, and ozone [19, 20]. Also, water isotope ratios are a powerful tool for testing general circulation models [21].

Most middle-atmosphere water isotope measurements so far have been carried out with satellite instruments that combine a large spatial coverage with a relatively low spatial resolution and a poor precision. High spatial and temporal resolution can be obtained by in situ balloon or aircraft instruments. However, there are very few in situ water isotope ratio measurements reported in the literature that achieve sufficient precision to test model hypotheses. Zahn et al. [22] used cold traps on board an aircraft to sample tropospheric air moisture at a height of 7 km. Analytical errors are reportedly ~ 25 ‰ for δ^2H and ~ 5 ‰ for δ^{18}O. Sampling times of 60 to 90 min led to a 'satellite-like' spatial resolution of ~ 500 km. Webster and Heymsfield [23] reported the first in situ water isotope ratio measurements with the Alias spectrometer on board a stratospheric airplane with good temporal (~ 20 s) and thus good spatial resolution (about 4 km for an airplane traveling at Mach 0.7). Analytical errors are reported as ~ 50 ‰ for all isotopes, and larger at low water concentration (< 10 ppmv). Franz and Röckmann [24] used a small-volume whole-air sampler in combination with a modified small-sample isotope ratio mass spectrometry (IRMS) analysis procedure [25] to obtain a precision of ~ 2 ‰ for the oxygen isotope ratio measurements. However, due to a strong correlation between the individual measurements, the ^{17}O anomaly, defined as $\Delta^{17}\mathrm{O} = \delta^{17}\mathrm{O} - 0.528\delta^{18}\mathrm{O}$, could be determined with a precision of 0.3 to 2 ‰, depending on the sample size. The sampling time was, depending on the water concentration, minimally 20 min, giving a spatial resolution > 240 km. Apart from the analytical precision, which may be quantified in the laboratory and determined from in situ data collected under conditions where little natural variation is expected, all instruments would have to be calibrated with international standards to assure a good accuracy. This is generally difficult to do under flight conditions and, in any event, possible fractionation in the air inlet introduces an almost inaccessible unknown systematic error. This makes intercomparison of different instruments (and inlet systems) an absolute must.

In this paper we report the development of an in situ near-infrared tunable diode laser spectrometer (Iris), based on ultra-sensitive optical feedback cavity-enhanced absorption spectroscopy (OF-CEAS) [26]. It measures all three water isotope ratios of interest, $^2\mathrm{H}/^1\mathrm{H}$, $^{17}\mathrm{O}/^{16}\mathrm{O}$, and $^{18}\mathrm{O}/^{16}\mathrm{O}$. A major advantage of Iris is the real-time, in situ measuring capability, providing a superior temporal (1 to 30 s) and spatial coverage, as well as easier logistics, albeit at the cost of a possibly reduced measurement accuracy, when compared to a cryogenic whole air sampling technique with laboratory isotope ratio analysis [24, 25]. In comparison to the Alias spectrometer built by Webster and colleagues [23], our design differs in several respects: Iris uses a near-infrared laser,

avoiding the need for cryogens, and it uses a variation of the cavity ring-down spectroscopy (CRDS) technique to achieve a substantially longer effective optical absorption path length (~ 6 km versus 80 m). Less fundamental, but more important from an atmospheric science perspective, is that Iris will be equipped with a particle-rejecting inlet, whereas Alias samples the total water content.

We are aware of only one other water isotope ratio spectrometer that has been flown on a high-altitude aircraft. This instrument, built by Moyer and colleagues [27], is, like ours, based on a CRDS technique, in this case called off-axis integrated cavity output spectroscopy (OA-ICOS), used in combination with a mid-infrared quantum cascade laser. The instrument is significantly larger and heavier than Iris, but has collected scientific-quality data during the July 2005 and February 2006 AVE missions.

The Groningen group has built water isotope spectrometers with a color-center laser as the light source (exciting the fundamental vibrational modes near 2.7 μm) [28], as well as with near-infrared diode lasers (around 1.4 μm) [29, 30], and has successfully used them in laboratory studies in biomedicine [31, 32], paleoclimatology [33], and ecology [34]. The spectrometers use two gas cells, each equipped with multiple-pass optics to achieve an effective optical absorption path length of ~ 20 m, one filled with the sample, the other with a reference material (which can be traced back to international isotope standards). Working at 1.4 μm, a state-of-the-art minimal detectable absorption of about 10^{-5} Hz$^{-1/2}$ means that the S/N of the recorded spectra is of the order of 10^4 Hz$^{-1/2}$ under typical sample conditions (10-μl liquid water injected in a 1-l volume, corresponding to a partial pressure of 13 mbar). However, when filled with arid air containing 10-ppmv water to a total pressure of 70 mbar, characteristic of upper troposphere or lower stratosphere conditions, such a spectrometer would register the stronger isotopologue features in the absorption spectrum with a S/N of only ~ 1 Hz$^{-1/2}$.

Increasing the sensitivity by increasing the effective absorption path length is limited to a factor of ~ 5, as the appearance of interference fringes poses a practical limit of about 100 m to the effective path length. An increase of the multipass path length leads almost inevitably to an even larger cell volume, increasing the time needed to exchange the gas-cell volume and thus reducing the temporal resolution of the instrument. For operation on an airborne platform, this translates into a reduced spatial resolution of the measurement.

In principle, another route towards an increased sensitivity would be to excite a ro-vibrational transition belonging to the stronger vibrational bands in the mid infrared, instead of the overtone and combination bands at 1.4 μm. This strategy was followed by Webster and Heymsfield [23]. However, in the case of water, the gain provided is only about one order of magnitude, and not much different for either of the bands near 2.7 μm or 6.7 μm. In fact, the overall gain that one can expect to achieve may well be much lower still, when taking into account the reduced performance of detectors at these wavelengths. Especially at 6.7 μm, the detectors will need to be cooled to very low temperatures to assure an acceptable detectivity. Also, high-reflectivity mirror coatings, required for the implementation of a cavity ring-down detection technique, are generally of lower quality (lower reflectivity and/or higher losses) at these wavelengths. As the name implies, in OA-ICOS, the laser beam traverses the gas cell along a beam path away from the symmetry axis of the cell. Consequently, the mirrors are required to be of much larger diameter than in a more conventional CRDS implementation. The instrument of Moyer and colleagues uses mirrors of about 10-cm diameter [27]. Not only are these difficult to manufacture to the required precision, but herewith the gas-cell volume becomes very large, too (roughly a factor of 10^3 larger than in our spectrometer). This means that a large flow needs to be maintained in order to bring the gas-exchange time down to an acceptable level and, ultimately, that the entire spectrometer becomes large.

To measure isotope ratios of trace amounts of water in the upper troposphere and lower stratosphere, our spectrometer was designed around the technique of OF-CEAS [26] used in combination with a thermo-electrically cooled diode laser emitting near 1.39 μm. In this way, a 100-fold increase in the effective optical path length is obtained, in comparison to the multiple-pass scheme, while at the same time the gas-cell volume is reduced by about the same factor. The gas cell exchange time can thus be kept to below 1 s, corresponding to a spatial resolution of 200 m (although longer averaging times may be needed to reach the required level of precision). The high gas-exchange rate is also critical in avoiding systematic errors due to contamination by tropospheric water. In this paper we focus on the design and laboratory performance of the spectrometer. In a forthcoming paper [35] we will present detailed results of the first airborne campaigns, which are beyond the scope of this paper.

2 Experimental

2.1 *Setup*

The principles of the OF-CEAS technique have recently been described in detail by Morville et al. [26]. Also, the first generation of our OF-CEAS water isotope ratio spectrometer, hereafter referred to as G2WIS, is rather similar to the device described by Romanini et al. [36] for measurement of the concentration of methane in ambient air down to the ppb level. Apart from the obvious difference in laser source (wavelength), a slightly different optical layout of the water isotope spectrometer assures that the spectrum is sampled at one-half the frequency spacing, enabling the spectrometer to resolve Doppler-limited absorption lines and thus to be operated at a lower gas pressure. Here we give only a brief description of our spectrometers, focusing on the items that are particular for the water isotope ratio instrument, and refer the reader to the previously mentioned papers for more detailed information. We start with the description of our first-generation spectrometer G2WIS. The paragraph following this outlines the modifications to the design that were deemed necessary to fly the new instrument (Iris) on a stratospheric airplane.

2.1.1 First-generation device: G2WIS. The spectrometer, schematically represented in Fig. 1a, consists of a V-shaped cavity with two equal-length arms of about 53 cm, which make a 2-degree angle with each other. The gas-cell is formed by two Pyrex tubes of 5-mm inner diameter leading from

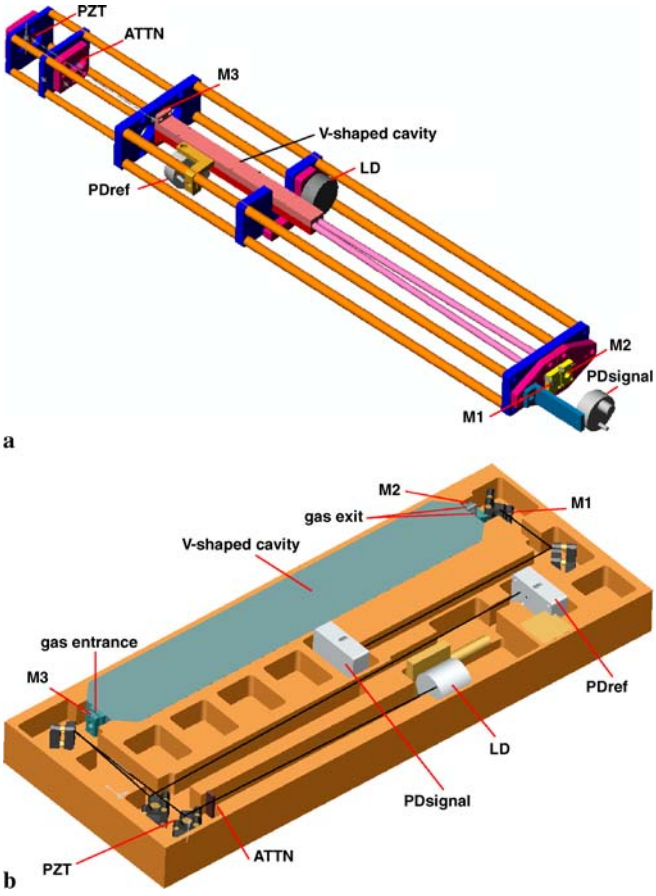

FIGURE 1 3-D views of the (**a**) G2WIS and (**b**) Iris optical layouts. LD = laser diode, PD = photodetector, PZT = piezo-mounted mirror, ATTN = attenuator, M1, M2 = cavity end mirrors, M3 = cavity folding mirror

the end mirrors to a stainless steel block with similar 5-mm channels machined inside that meet just in front of the folding mirror at the cavity apex, located at the other end of this block. The mirror holders are supported by a light frame around the cavity, built from aluminum plates and steel rods. The entire cavity and associated optics (the 'optical head') weighs less than 5 kg. The cavity mirrors are from Layertec GmbH. The plano-concave substrates with a radius of 1 m are slightly wedged and the mirror transmission was measured to be $(1.6 \pm 0.1) \times 10^{-5}$, while the measured ring-down time for the evacuated cavity (20.5 μs) then implies a loss coefficient (absorption and scattering) of $(6.5 \pm 0.2) \times 10^{-5}$. The laser source is a distributed feedback (DFB) diode laser emitting up to 10 mW at 1392 nm (LaserComponents). A home-built temperature controller stabilizes the laser temperature with 1 mK precision and better than 100 mK accuracy, assuring that the spectral region of interest is accurately recovered and subsequently maintained after power turn-on. The laser beam is mode matched to the cavity by slightly focusing the beam with a high numerical aperture, aspheric lens. The beam passes through a linear polarizer, used to control the amount of feedback to the laser, before part of the beam is picked off a wedged beam splitter to monitor the instantaneous laser power with a room-temperature InGaAs detector. A piezo-mounted steering mirror then directs the laser beam to the cavity (apex) folding mirror. The low-voltage piezo is part of a relatively slow control loop (30-Hz bandwidth) that optimizes the phase of the laser field returning to the laser from inside the cavity (at resonance). This phase is controlled by adjusting the laser–cavity distance, thus assuring effective injection of light into the cavity by optimizing the optical feedback locking effect. The error signal for the control loop is derived from the symmetry of the transmitted signal patterns which correspond to the cavity modes in the presence of optical feedback locking, as explained in more detail in Morville et al. [26]. The cavity transmission is monitored by another InGaAs detector placed after one of the two end mirrors. Both detectors have a transimpedance gain of 4.7×10^5 V/A and a bandwidth of 160 kHz (Thorlabs PDA400).

The laser–cavity distance matches the length of the cavity arms. It can be shown [26] that in this case the OF-CEAS absorption spectrum is sampled at all the longitudinal cavity modes spaced in frequency by exactly one cavity free spectral range (FSR, 141.5 MHz in this case). The methane spectrometer mentioned before has a laser–cavity distance that is twice as large, in which case one can show that only every other longitudinal cavity mode contributes to the OF-CEAS spectrum. This can be a favorable configuration if relatively broad absorptions are to be recorded. Such was the case for the methane spectrometer, which operated at a gas pressure of 400 mbar. The water isotope spectrometer is, however, designed to operate at altitudes of around 20 km, or atmospheric pressures as low as 60 mbar. In order to avoid the necessity of a compressor before the cavity, which would have a detrimental effect on the system's time response, we instead elected to sample the spectra with the smallest possible frequency spacing. A minor disadvantage of the current scheme is that cavity modes for which the distance between the end mirrors differs by one half wavelength, referred to as the even- and odd-mode families, experience a slightly different reflection coefficient at the folding mirror [26]. This results in a slight offset between the spectra registered by the odd and even modes, respectively (see below).

The gas enters the cavity near the folding mirror and is able to exit the cavity near both end mirrors, after which the flow is recombined. The pressure inside the cavity is regulated to a constant value set between 40 and 70 mbar by a pressure controller placed before the cavity (Bronkhorst P602), while a needle valve immediately after the cavity regulates the flow to typically 800 ml/min STP. Together with the volume of the cavity (between the mirrors) of about 16 ml, this leads to a very short gas-exchange time of roughly 0.1 s, greatly reducing memory effects due to water adsorption onto the gas-cell walls.

The instrument is controlled by a C program running on a 2.4-GHz Pentium 4, 19-in, rack-mounted, industrial computer (ADlink RK-410S-NuPro840LV), interfaced to the spectrometer through a multi-function data-acquisition card (ADlink DAQ-2010; 14-bit simultaneous sampling ADC, 12-bit DAC, 24-bit DIO, and two 16-bit timers). Both the reference and the transmission signal photodetector outputs are digitized at a rate of 200 kHz for a record length of 16 k data points during normal spectra registration. The laser injection current is ramped at a rate corresponding to one mode (cavity FSR) per 0.51 ms, or about 0.75 cm^{-1} per spectrum of

Isotopologue	Position (cm^{-1})	Vibrational band	Rotational assignment	Ground-state energy (cm^{-1})	Temperature coefficient (‰/K)
$H^{18}OH$	7183.58594	$\nu_1+\nu_3$	$5_{51} \leftarrow 5_{50}$	733.7	+6.9
$H^{16}OH$	7183.68604	$2\nu_3$	$5_{24} \leftarrow 6_{33}$	661.5	+5.7
$H^{17}OH$	7183.73535	$\nu_1+\nu_3$	$1_{10} \leftarrow 2_{11}$	95.0	−3.4
$H^{16}OD$	7183.97266	$2\nu_3$	$3_{03} \leftarrow 4_{14}$	156.4	−2.5
$H^{16}OH$	7184.10107	$2\nu_3$	$9_{63} \leftarrow 9_{72}$	1810.6	+26.8

TABLE 1 List of the absorption lines observed in this work. Line positions and assignments were taken from the HITRAN 2004 database [39]. The temperature coefficients were evaluated at 296 K. The first four lines are used for the isotope ratio determinations, while the last ($H^{16}OH$) line is used in combination with the first $H^{16}OH$ line as an internal gas thermometer

160 modes. Ring-down events are recorded with a digitization rate of 1 MHz for a total time approximately 10 times longer than a typical ring-down time of 20 µs. Processing of the data is largely done in real time: division of the cavity transmission signal by the reference signal, locating the maxima of all modes in the scan, and conversion of the cavity transmission to absolute absorption units, in a manner as discussed in the following paragraphs. The overall data-acquisition rate amounts to about eight to 10 spectra per second. The conversion to absolute absorption units is made using the ring-down time determined for one preselected mode in the spectrum, once every 10 spectra (roughly once per second). For this measurement, the laser is abruptly turned off at the top of the cavity transmission for that mode, enabling the subsequent ring-down event to be recorded by the signal photodetector. Fitting of the spectra to the sum of a number of line profiles (including motional (Wittke and Dicke [37]) narrowing using the Rautian–Sobel'man hard collision model [38]) is done off-line. The off-line processing time is about equal to the total data-acquisition time.

The optical head is mounted inside an aluminum enclosure measuring approximately 90 cm by 16 cm by 16 cm, of which both the inside and the outside walls are covered with thermal isolation foam. Ribbon heaters controlled by a platinum resistance temperature detector in combination with simple on/off electronics (Minco CT325) maintain the set temperature (30 °C) to within ±0.5 °C. This temperature stability is more than sufficient to avoid any noticeable misalignment of the optics. However, it is only marginally sufficient to avoid temperature-induced drifts in the apparent isotope ratios. This is because the line strength depends on the number of molecules in the lower level of the transition: a change in temperature will redistribute the population over the rotational levels of the ground vibrational state (for an in-depth discussion of the effect of temperature on isotope ratio measurements, see e.g. [16]). In fact, the selected lines, listed in Table 1, show intensity temperature coefficients of several per mil per degree °C. The temperature coefficient of the isotope ratio (or rather the associated δ value) is to a good approximation equal to the difference of the temperature coefficients of the rare and abundant isotopologue lines. In our case, the isotope ratio temperature coefficients are thus +1.2 ‰/K, −9.1 ‰/K, and −8.2 ‰/K, for the $\delta^{18}O$, $\delta^{17}O$, and δD isotope ratios, respectively. The region scanned by the laser contains a second $H^{16}OH$ line with a substantially different intensity temperature coefficient. The intensity ratio of the two $H^{16}OH$ lines may be used as an internal gas temperature sensor with a sensitivity of 21.1 ‰/K. The precision with which this intensity ratio can be determined is approximately equal to that of the $^{18}O/^{16}O$ isotope ratio. Considering that the measurement precisions for $\delta^{17}O$ and $\delta^{2}H$ are inferior to the ^{18}O precision, we expect that, ultimately, temperature-induced drifts can be corrected to a level well below the measurement precision for each of the three isotopes.

2.1.2 Second-generation device: Iris. An improved version of the instrument described above was built to make the design compatible with flights on NASA's WB-57F high-altitude airplane. Most importantly, the industrial computer was not designed to withstand operation at reduced pressure and was therefore replaced by PC104 form-factor hardware (RTD Embedded Systems ARC01-HiDAN-SYS104 with CML36786HX 1-GHz clock speed CPU module and two ACCES I/O 104-AIO-1616W multi-function boards with 16-bit analog inputs) with a typical power consumption of less than 20 W. Data acquisition using the 16-bit analog inputs of the multi-function boards is performed at a rate of 250 kHz for the normal spectra scans, and 500 kHz for the registration of the ring-down event. Unfortunately, the ACCES data-acquisition boards did not allow fast data transfer to the PC memory and every other laser scan is lost, reducing the effective spectra acquisition rate to about 4 Hz. The optical layout was changed in order to reduce the overall length of the instrument and to reduce the sensitivity to mechanical vibrations. The instrument is therefore built on a 50-mm-thick aluminum plate, measuring 64 cm by 34 cm, with material milled out so that all optical elements are recessed and the laser beam travels in a plane 35 mm above the bottom surface of the plate. Insensitivity to mechanical vibrations was further improved by increasing the bandwidth of the feedback loop, which controls the phase of the laser field at the folding mirror, from 30 to 80 Hz. The smaller footprint allowed the instrument to be fitted underneath an existing instrument (the Argus tunable diode laser spectrometer) in one of the bay pallets of the WB-57F. The ribbon heaters are glued directly to the aluminum base plate, improving heat distribution and thus reducing temperature gradients in the system. In the new layout, the V-shaped cavity is made by machining grooves with half-circular cross section into a solid stainless steel block, and sandwiching two identical blocks together. The inside of the cavity is mirror polished. The mirror holders are no longer equipped with fine-pitch screws. Instead, the mirrors are pre-aligned on a red laser beam and glued in place onto mirror holders that can be removed for mirror-cleaning purposes, and replaced without affecting the optical alignment. Figure 1b gives a 3-D outline of the Iris optical head.

New cavity mirrors were acquired (Layertec GmbH) with essentially the same reflectivity, but with significantly increased transmission ($T \approx L$). Finally, the photodetectors were replaced by amplified 0.3-mm-diameter InGaAs detectors (Redwave Ltd.) with a larger bandwidth, but reduced

noise and gain to accommodate the approximately three times larger photon fluxes compared to the G2WIS device.

2.2 *Data analysis: from raw signals to absorption spectra*

In order to determine the isotope ratios, we want to determine the molecular absorption coefficient α (or the absorbance a), as it is the absorption coefficient that is directly proportional to the absorber number density n:

$$\alpha = \frac{a}{l} = Sf(0)n\,, \tag{2}$$

where S is the line strength, $f(0)$ the normalized line-shape function evaluated at the center-line frequency, and l the absorption path length. In a direct absorption detection scheme, α is, in principle, obtained in a very straightforward manner as $\alpha = -(1/l)\ln(I_t/I_0)$, with I_t the transmitted intensity and I_0 the incoming light intensity (Lambert–Beer–Bouguer law).

The situation in the case of optical feedback CEAS is more complicated, but of fundamental importance for the measurement of isotope ratios on a linear scale over a relatively wide range, such as we expect to encounter in the stratosphere. The intensity at the output mirror of the cavity, when illuminated by a very narrow bandwidth laser source, is obtained by considering the superposition of the amplitudes of the fields transmitted by the cavity. It can be shown that for a V-shaped cavity with cavity arm lengths l_1 and l_2, the presence of an absorber, with absorption coefficient $\alpha_m = \alpha(\omega_m)$ at the center of a cavity mode, leads to an Airy-shaped cavity transmission transfer function whose maxima at frequency ω_m are given by [26]

$$H_{\max}(\alpha_m) = \left[\frac{T\mathrm{e}^{-\alpha_m l_1/2}}{1-R^2\mathrm{e}^{-\alpha_m(l_1+l_2)}}\right]^2 . \tag{3}$$

Here, T and R represent, respectively, the effective mirror transmission and reflectivity coefficients: $T = (T_v T_1)^{1/2}$ and $R = (R_v)^{1/2}(R_1 R_2)^{1/4}$, where the subscript v refers to the folding (apex) mirror and 1 and 2 are the subscripts of the (end) mirrors in arms 1 and 2 of the V-cavity (the transmitted intensity being observed behind mirror 1). Since all three mirrors will normally come from the same coating batch, the coefficients are expected to be practically indistinguishable. However, the laser beam strikes the folding mirror under a slight angle away from normal ($\sim 2°$), which will alter the coefficients of this mirror to some extent. Conservation of energy requires then that the effective mirror losses (absorption and scattering) are given by $L = 1 - R - T$. Equation (3) is valid in the case of cavity injection by a perfectly monochromatic field slowly passing through the resonance. In our case, this condition is fulfilled due to the fact that a full cavity buildup occurs during frequency locking by optical feedback, which at the same time induces a laser line width narrowing to below the cavity mode width. The maximum transmission of the empty cavity is approximately equal to $0.25(1 + (L/T))^{-2}$, which approaches 25% for a completely lossless cavity ($\alpha_m = 0$ and $L \equiv 1 - R - T = 0$). It should be noted that (3) is derived by squaring the sum of the amplitudes of the field leaking out of one of the arms of the cavity, instead of summing the square of the amplitudes [26]. The latter (intensity-summing) case is only valid in the case of a broadband incoherent source and results in a substantially lower transmission, with a maximum value of only $T/4$ for the V-shaped cavity. Inversion of (3) is straightforward if we neglect the term $\exp(-\alpha_m l_1) \approx 1$ in the numerator:

$$\alpha_m = \frac{1}{l_1+l_2}\left\{2\ln(R) - \ln\left(1 - \frac{T}{\sqrt{H_{\max}}}\right)\right\} . \tag{4}$$

The peak cavity transmission $H_{\max}(m)$ for each cavity mode m is obtained as the maximum of the ratio of the cavity output signal over the cavity input signal. This normalization is necessary as the laser power increases during a frequency sweep (induced by a current ramp) and also suffers small ($\sim 1\%$) transient variations during frequency locking. In principle, the mirror coefficients R and T have to be known in order to calculate α_m from the measured $H_{\max}(m)$ values.

In the following, we will show that it is possible to obtain the absorption spectrum directly, using the result of only one ring-down measurement carried out for a given cavity mode k in the scan. In fact, given the approximation $T/\sqrt{H_{\max}} \ll 1$ (which is very good considering that in most practical cases very large absorptions are avoided, such that $H_{\max} > 0.01$), we can write

$$\alpha_k \approx \frac{2}{l_1+l_2}\ln(R) + \frac{T}{(l_1+l_2)\sqrt{H_{\max}(k)}}\,, \tag{5}$$

and recognize that the first term on the right is just $-\gamma_0$, (minus) the loss per unit length for the empty cavity (evident if we write $-\ln(R) \approx 1 - R = T + L$), which may be grouped with α_k:

$$\frac{\gamma_k}{c} = \alpha_k - \frac{2}{l_1+l_2}\ln(R) = \alpha_k + \frac{\gamma_0}{c} \approx \frac{T}{(l_1+l_2)\sqrt{H_{\max}(k)}}\,, \tag{6}$$

where the total loss coefficient γ_k may be determined experimentally by fitting $\exp(-\gamma_k t)$ to a ring-down event, produced by abruptly turning off the laser at ω_k, i.e. after injection of mode k to the maximum intensity. The CEAS spectrum is then obtained in absolute absorption units, apart from a constant offset γ_0 (corresponding to the empty cavity losses, just as in CRDS), simply by calculating $1/\sqrt{H_{\max}(m)}$ for all the modes m and then multiplying by the 'ring-down factor' $(\gamma_k/c)\sqrt{H_{\max}(k)}$ obtained for the given mode k.

This absorption-scale calibration procedure has the major advantage that it may be performed even in the presence of intracavity absorption. Perhaps counter-intuitively, quantitative CEAS measurements do not depend on a measurement of the ring-down time for an empty cavity or for a cavity filled with a non-absorbing buffer gas. This is clearly of importance for the precise retrieval of absorption-line intensities as needed to calculate molecular concentrations. In fact, the determination of the absolute absorbance in the case of 'simple' direct absorption is by far not as trivial as (2) could lead one to think. Apart from the requirement to accurately measure the effective absorption-path length, there is the issue of accounting for the scattering and absorption occurring in the gas-cell windows. The first problem could be dealt with by interferometrically measuring the distance between the gas-cell windows (see e.g. [40]); the second almost inevitably

requires the registration of an empty gas cell spectrum within a time frame imposed by the stability of the spectrometer, typically shorter than one minute (see e.g. [41] and references therein).

It is important to note that, even though (5) and (6) are not exact, the error is zero at the absorption coefficient at which the ring-down event was measured. In any case, since for an actual absorption measurement the difference between the (center-)line absorption and the background is evaluated, the relative error in the line-intensity determination remains very small up to large absorptions (smaller than 0.3 per mil for mirror parameters appropriate for our cavity), assuring a very linear scale.

The discussion so far has ignored the fact that the value of $H_{\max}(m)$ returned by the CEAS measurements is accurate to a scaling factor θ, mainly due to the fact that the reference photodetector output is proportional to the total power in the incoming laser beam, whereas only part of this is used to excite the TEM_{00} mode of the cavity. The resulting scaling error is eliminated in the normalization procedure as it has practically the same value for all modes, and is in any case expected to be highly reproducible, thus not affecting the final isotope ratio precision.

Since cavity injection by optical feedback is efficient, and light transmission at the peak of a cavity mode is high, ring-down signals are obtained with excellent S/N and we may recover γ_k to better than 0.1% in a single measurement. In particular, we observe in our setup that the shot-to-shot standard deviation of ring down rate measurements (obtained for the same cavity mode over successive laser scans) coincides with the standard deviation of the ring-down rate given by the fit. This implies that we are limited by the intrinsic noise on the digitized ring-down signal, mostly photodetector and digitization noise. Since the S/N ratio also exceeds 10^3 for the determination of the $H_{\max}(m)$ values, the scaling factor is precise and reproducible to better than $\sim 0.1\%$. Given a cavity finesse of around 20 000, this corresponds to a detection limit of a few times $10^{-10}\,\mathrm{cm}^{-1}\,\mathrm{Hz}^{-1/2}$ for the absorption coefficient. As we will see below, we obtain this performance on short time scales, but all data presented here are limited by residual interference fringes superimposed on the spectra, which introduce small errors in the line intensities obtained from fits to line profiles. As the fringes drift in time, these errors also drift in time and produce long-term variations, of roughly 0.3% for the present case. The cause of fringes has been traced to back-reflections from the photodetectors. In the latest version of Iris the fringes are practically eliminated by tilting the detectors away from normal incidence and by the use of an optical isolator just before the cavity output detector.

3 Results and discussion

3.1 *Spectrum and isotope ratio determination*

Figure 2 gives an example of a spectrum recorded with the G2WIS spectrometer in about 1 s. The 1σ noise on the residuals of the fit indicates a detection limit of $4 \times 10^{-10}\,\mathrm{cm}^{-1}\,\mathrm{Hz}^{-1/2}$.

During the off-line fitting process, only one Doppler-width parameter is included, but the Doppler widths of the

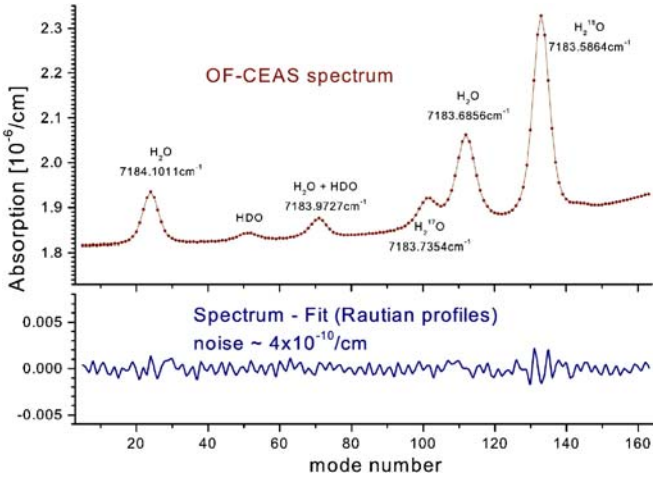

FIGURE 2 OF-CEAS spectrum recorded with the first-generation G2WIS spectrometer at a water concentration of approximately 600 ppmv

individual lines are scaled with the square root of the isotopologue mass. For spectra with low S/N (i.e. a water concentration below about 100 ppm), a fitting model is used where the relative distances between the lines are kept fixed to the corresponding values retrieved from high-quality, high water concentration spectra (such as the one in Fig. 2). The same is done for the line-width and collisional narrowing parameters. This is allowed because of the practically perfect equidistant sampling of the spectrum in frequency space. These procedures greatly improve the robustness, speed, and quality of the fits, especially for low signal strengths, without affecting the standard deviation of the fit. In addition, the spectra belonging to the odd and even cavity modes are superimposed by including a parameter in the spectral fit model that represents the difference in the empty cavity loss terms γ_0^{even} and γ_0^{odd} for the even and odd modes. Finally, the spectrum baseline is fitted using just a constant bias plus the Lorentzian wing of a strong water absorption line which lies outside the spectral window and whose position and width are fixed while its intensity is adjusted during the fit. This baseline model accounts perfectly for the curvature and slope clearly visible in Fig. 2, and this fact argues clearly for the excellent precision of the data obtained by OF-CEAS. The isotope ratios (or rather the δ values) are calculated using an analytical expression for the area under the line profiles.

Without the inclusion of motional (Dicke) narrowing, the noise on the residuals of the spectrum in Fig. 2 increases to $5 \times 10^{-10}\,\mathrm{cm}^{-1}$. This seems a modest increase. However, the actual improvement in the fit is better than this number suggests, considering that the residuals on the $H^{18}OH$ line are believed to have a different origin. A recent ab initio calculation of the water spectrum by Schwenke and Partridge [42, 43] concluded that the $H^{18}OH$ feature observed here is in fact a doublet, a result that appears to be supported by our data. We do not attempt to fit the doublet for purposes of isotope ratio determinations, as this results in a set of strongly correlated parameters. Since the doublet originates from the same ground state, it behaves as one line as far as its temperature coefficient is concerned.

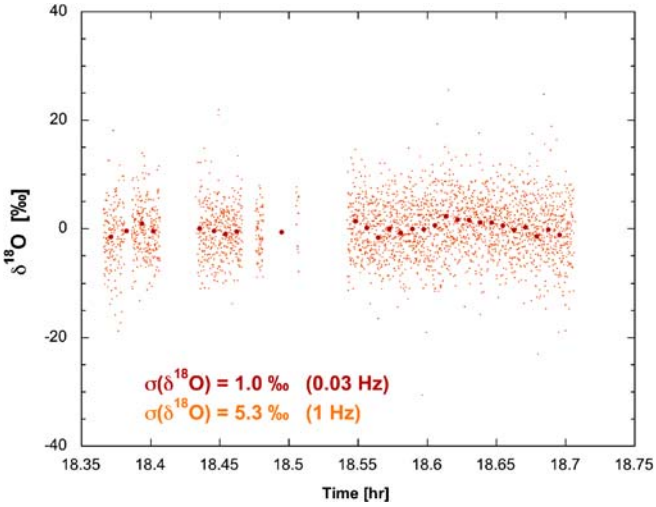

FIGURE 3 Precision of the δ^{18}O measurement during tropospheric flight of G2WIS

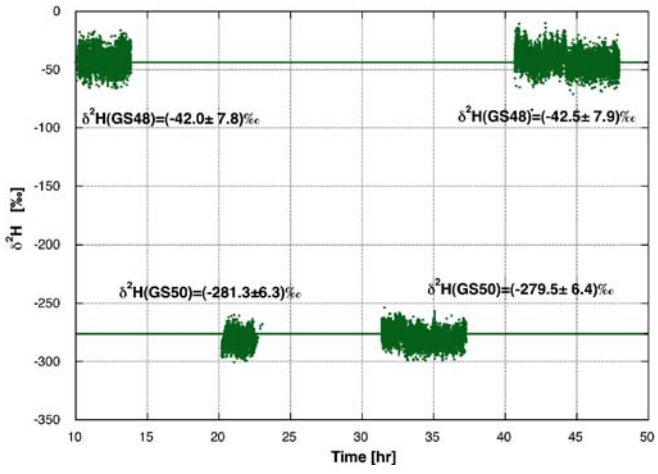

FIGURE 4 δ^2H values measured with G2WIS (1-s bandwidth). The numbers next to each sample measurement give the average value and standard deviation of the measurement in question, as determined by the optical spectrometer. The isotope ratios of the standards with respect to VSMOW, determined by IRMS analyses, are δ^{18}O(GS48) = −6.46 ‰, δ^2H(GS48) = −43.3 ‰, δ^{18}O(GS50) = −35.06 ‰, and δ^2H(GS50) = −276.7 ‰. The IRMS values (*solid lines*) are recovered by the optical spectrometer to within the 1σ standard deviations

3.2 *Measurement precision*

In Fig. 3 we show results of ^{18}O isotope ratio determinations carried out on board NASA's DC-8 in Dryden, California. The time series of the figure covers a time span of about 20 min during which the airplane flew at a constant altitude of 13 km, sampling a constant water vapor concentration and, we assume, constant isotope ratios. The effective data-acquisition rate was ∼ 5 spectra per second, limited by a hardware bottleneck in streaming data to disk, which has since been resolved. The 1σ standard deviation amounts to 5.3 ‰ for the δ values calculated from the spectra for an effective data-acquisition bandwidth of 1 Hz, while averaging ('binning') 30 δ values reduces the standard deviation to 1.0 ‰ (0.03-Hz bandwidth). The water mixing ratio was estimated to be ∼ 200 ppm, mostly determined by a small leak in the gas-inlet system. For this reason, no attempt was made to determine an absolute δ^{18}O value. Instead, the [H^{18}OH]/[H^{16}OH] ratio determined for an earlier section of the time series was used as $^{18}R_{\text{reference}}$ in the expression of (1). In a similar manner the 1σ standard deviations were determined for δ^{17}O (16 ‰ and 2.8 ‰ for no averaging and averaging of 100 measurements, respectively) and δ^2H (64 ‰ and 8.5 ‰). This performance is not different from what we obtained in the laboratory with the same instrument. The gaps visible in Fig. 2 were caused by operator interventions. As the feedback loop that controls the phase of the laser field at the folding mirror occasionally unlocked, different settings of the electronics were tried in-flight.

3.3 *Calibration and time response*

A series of measurements were carried out in which two different air samples were alternately led through the G2WIS device. The samples were prepared by bringing liquid-water samples of known isotopic composition (the GS-48 and GS-50 laboratory standards of the Groningen Center for Isotope Research) in preconditioned 50-l tanks, filled to 1 bar with a dry synthetic air mixture, and subsequently filling these tanks further with synthetic air to a total pressure of about 40 bar. The water mixing ratios are approximately 300 ppmv. The flow rate was adjusted to 250 ml/min and the pressure controller before the cavity was set to 80 mbar. As we could not be sure that no isotope fractionation would occur, e.g. by wall effects in the tanks, we re-collected the water by cryogenic trapping after it passed through the spectrometer.

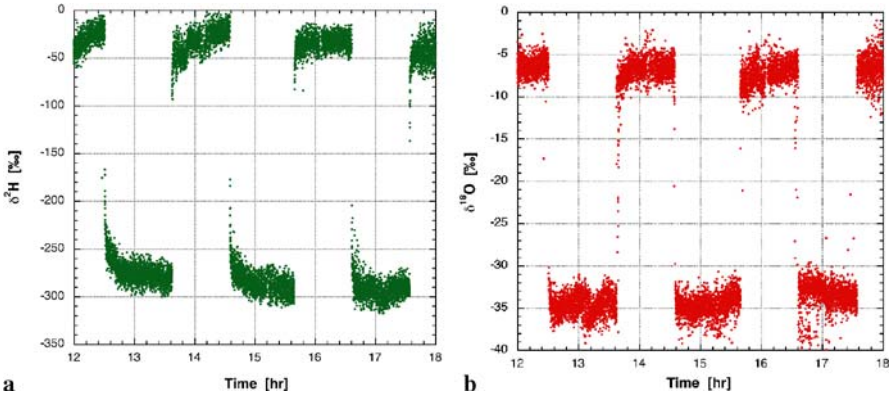

FIGURE 5 (**a**) δ^2H and (**b**) δ^{18}O measurements with repeated switching between the two air samples with different water isotope ratios. Samples and conditions are the same as for Fig. 4

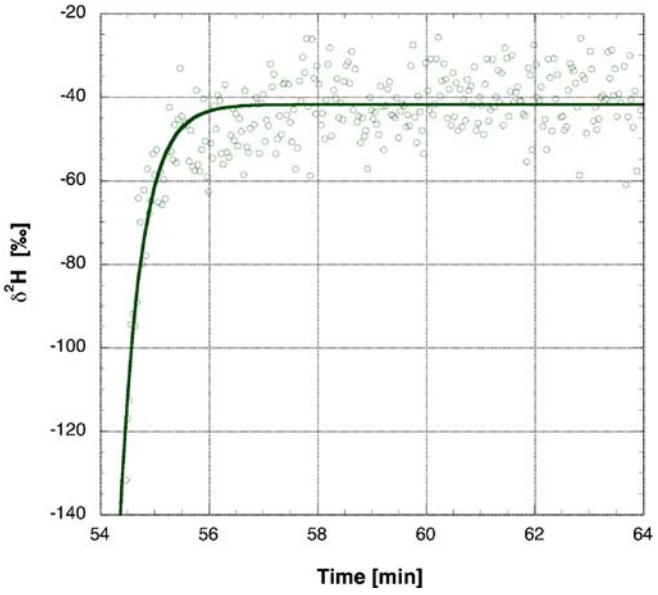

FIGURE 6 δ^2H time response of G2WIS: a single-exponential fit to the data (*solid line*) reveals a time constant of 24 s

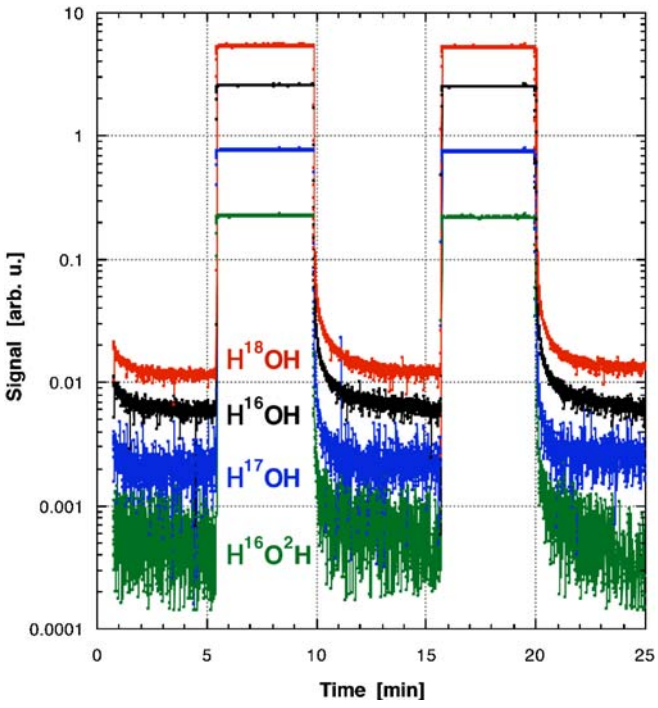

FIGURE 7 Time response of Iris: the $H^{18}OH$ signal following the switch from ambient air to dry air was fitted using a double exponential with time constants of 0.29 s and 3.4 s. On the inverse transition all signals follow with a single-exponential time constant smaller than 2 s

These samples were independently analyzed by IRMS for δ^{18}O and δ^2H. The optical spectrometer was calibrated by fixing the average measured isotope ratios of an initial 2-h-long time measurement of GS-48 (not shown in the figure) to their consensus (IRMS) values. Figure 4 demonstrates that subsequent G2WIS and IRMS measurements of the isotopic ratios agree to within the measurement precision. In fact, the difference in the GS-48 and GS-50 isotope ratios is, if anything, overestimated (238.1 ‰ versus 233.4 ‰ by IRMS): where memory effects would have produced a scale contraction, we actually observe a slight scale expansion.

The same measurements were repeated without cryogenically trapping the exiting water. These measurements are shown in Fig. 5. Here the flows coming from the two tanks can be switched on a time scale of a few seconds, enabling a registration of the time response of the device.

The result of an exponential fit to the last transition in the δ^2H data of Fig. 5 is shown in Fig. 6. A time constant of 24 s is deduced in this manner.

Finally, in Fig. 7 we show the time response of the second-generation device Iris. In order to demonstrate the dynamic range of the spectrometer, the instrument was switched between room air and dry nitrogen (containing approximately 10-ppm water). The noise visible during the measurement of room air is caused by the fact that the sample is now nearly optically black. Despite the almost three orders of magnitude difference in water mixing ratio, the signals follow the switch in flow with a time constant of less than 2 s. We can thus be fairly confident that Iris will indeed be able to measure stratospheric isotope ratios and not suffer from tropospheric contamination.

4 Conclusions

We have described a sensitive water isotope ratio spectrometer that was developed for airborne operation. The instrument is lightweight (45 kg) and small (< 50 l). Together with a low power consumption and the absence of cryogens, this makes it uniquely suited for operation on unmanned aerial vehicles and high-altitude aircraft. It was first tested on the NASA DC-8 in 2004. Under conditions typical of the middle to upper troposphere, a precision was demonstrated of 1 ‰, 3 ‰, and 9 ‰ for δ^{18}O, δ^{17}O, and δ^2H, respectively (30-s averaged data). With recent improvements to the newly designed stratospheric version of the Iris spectrometer, in particular the elimination of optical fringes and the use of lower-loss mirrors, we hope to achieve a performance that remains within a factor of three of the above values for water mixing ratios typical of stratospheric conditions (< 10 ppmv). Even for the case of deuterium, such a performance is sufficient to reveal interesting isotope dynamics in the upper troposphere/lower stratosphere, considering the large variation in atmospheric water isotope ratios (several 100 per mil for δ^2H, several 10 per mil for the oxygen isotope ratios). Unfortunately, we have not yet been able to demonstrate this in practice, due to minor electrical failures during recent (piggyback) test flights on the WB-57F high-altitude research aircraft.

Although cavity ring down is used to calibrate the absolute absorption measurement of the spectrometer, this is not a substitute for proper in situ calibration to water isotope standards. Therefore, it would be of great scientific interest to compare the time series obtained by our instrument with the off-line, low time resolution, but potentially more precise, whole air cryogenic sampling device of Franz and Röckmann [25], as well as with the other two existing stratospheric water isotope spectrometers [23, 27]. Such an intercomparison between (fundamentally) different measurement techniques is obviously of great importance to assess the quality of the data sets.

ACKNOWLEDGEMENTS This work would have been impossible without the expert technical assistance of Henk Been, Bruce Borchers, and Jim Terman. The project was funded by the Dutch Foundation for Fundamental Research on Matter (FOM) under Contract No. 99MAP10. Additional financial support was obtained in the form of University of Groningen Strategic Funding, internal funding by the Center for Isotope Research, as well as a NASA Ames Directors Discretionary Fund. E.R.T.K. is grateful to the Royal Netherlands Academy of Arts and Sciences (KNAW) for a 5-year young investigator fellowship. Finally, we thank three anonymous reviewers for helpful comments on the manuscript.

REFERENCES

1 J. Lelieveld, P.J. Crutzen, Nature **343**, 227 (1990)
2 J. Lelieveld, P.J. Crutzen, Science **264**, 1759 (1994)
3 R.G. Prinn, in *Treatise on Geochemistry*, Vol. 4, *The Atmosphere*, ed. by R.F. Keeling (Elsevier, Amsterdam, 2004), Chap. 1, pp. 1–19
4 A. Stenke, V. Grewe, Atmosph. Chem. Phys. **5**, 1257 (2005)
5 S.J. Oltmans, H. Vomel, D.J. Hofmann, K.H. Rosenlof, D. Kley, Geophys. Res. Lett. **27**, 3453 (2000)
6 K.H. Rosenlof, E.W. Chiou, W.P. Chu, D.G. Johnson, K.K. Kelly, M.H. Michelsen, G.E. Nedoluha, E.E. Remsberg, G.C. Toon, M.P. McCormick, Geophys. Res. Lett. **28**, 1195 (2001)
7 W. Randel, F. Wu, S. Oltmans, K. Rosenlof, G. Nedoluha, J. Atmosph. Sci. **61**, 2133 (2004)
8 K.H. Rosenlof, J. Meteorol. Soc. Jpn. **80**, 831 (2002)
9 T. Röckmann, T. Rhee, A. Engel, Atmosph. Chem. Phys. Discuss. **3**, 3745 (2003)
10 T. Röckmann, J. Grooss, R. Miller, Atmosph. Chem. Phys. **4**, 693 (2004)
11 S.C. Sherwood, A.E. Dessler, Atmosph. Chem. Phys. **3**, 4489 (2003)
12 S.C. Sherwood, A.E. Dessler, Geophys. Res. Lett. **27**, 2513 (2000)
13 S.C. Sherwood, A.E. Dessler, J. Atmosph. Sci. **58**, 765 (2001)
14 J.R. Holton, A. Gettelman, Geophys. Res. Lett. **28**, 2799 (2001)
15 E.J. Jensen, L. Pfister, A.S. Ackerman, A. Tabazadeh, O.B. Toon, J. Geophys. Res. **106**, 17 237 (2001)
16 E.R.T. Kerstel, in *Handbook of Stable Isotope Analytical Techniques*, ed. by P.A. de Groot (Elsevier, Amsterdam, 2004), pp. 759–787
17 B. Toon, E. Jensen, J. Holton, J. Logan, P. Newman, R. Salawitch, D. Starr, D. Waugh, P. Wennberg, *Draft of Tropical Composition, Cloud and Climate Coupling Experiment (TC4)* (NASA Goddard Space Flight Center, MD, 2003)
18 H.A.J. Meijer, W. Li, Isotopes Environ. Health Stud. **34**, 349 (1998)
19 J.R. Lyons, Geophys. Res. Lett. **28**, 3231 (2001)
20 C. Bechtel, A. Zahn, Atmosph. Chem. Phys. Discuss. **3**, 3991 (2003)
21 D.G. Johnson, K.W. Jucks, W.A. Traub, K.V. Chance, J. Geophys. Res. D **106**, 12 219 (2001)
22 A. Zahn, V. Barth, K. Pfeilsticker, U. Platt, J. Atmosph. Chem. **30**, 25 (1998)
23 C.R. Webster, A. Heymsfield, Science **302**, 1742 (2003)
24 P. Franz, T. Röckmann, Atmosph. Chem. Phys. **5**, 2949 (2005)
25 P. Franz, T. Röckmann, Rapid Commun. Mass Spectrom. **18**, 1429 (2004)
26 J. Morville, S. Kassi, M. Chenevier, D. Romanini, Appl. Phys. B **80**, 1027 (2005)
27 E.J. Moyer, T.F. Hanisco, F.N. Keutsch, D.M. Sayres, N.T. Allen, J.M.S. Clair, E.M. Weinstock, J.R. Spackman, J.B. Smith, L. Pfister, T.P. Bui, J.G. Anderson, unpublished (2006)
28 E.R.T. Kerstel, R. van Trigt, N. Dam, J. Reuss, H.A.J. Meijer, Anal. Chem. **71**, 5297 (1999)
29 E.R.T. Kerstel, G. Gagliardi, L. Gianfrani, H.A.J. Meijer, R. van Trigt, R. Ramaker, Spectrochim. Acta A **58**, 2389 (2002)
30 L. Gianfrani, G. Gagliardi, M. van Burgel, E.R.T. Kerstel, Opt. Express **11**, 1566 (2003)
31 R. van Trigt, E.R.T. Kerstel, R.E.M. Neubert, H.A.J. Meijer, M. McLean, G.H. Visser, J. Appl. Physiol. **93**, 2147 (2002)
32 E. Kerstel, T. Piersma, J. Gessaman, A. Dekinga, H. Meijer, H. Visser, Isotopes Environ. Health Stud. **42**, 1 (2006)
33 R. van Trigt, H.A.J. Meijer, A.E. Sveinbjornsdottir, S.J. Johnsen, E.R.T. Kerstel, Ann. Glaciol. **35**, 125 (2002)
34 E.R.T. Kerstel, L.G. van der Wel, H.A.J. Meijer, Isotopes Environ. Health Stud. **41**, 207 (2005)
35 H.J. Jost, R. Iannone, D. Romanini, M. Chenevier, S. Kassi, E. Kerstel, unplublished (2006)
36 D. Romanini, M. Chenevier, S. Kassi, M. Schmidt, C. Valant, M. Ramonet, J. Lopez, H.-J. Jost, Appl. Phys. B **83**, 659 (2006)
37 J.P. Wittke, R.H. Dicke, Phys. Rev. **103**, 620 (1956)
38 S.G. Rautian, I.I. Sobel'man, Sov. Phys. Uspekhi **9**, 701 (1967)
39 L.S. Rothman, D. Jacquemart, A. Barbe, D.C. Benner, M. Birk, L.R. Brown, M.R. Carleer, C. Chackerian Jr., K. Chance, L.H. Coudert, V. Dana, V.M. Devi, J.-M. Flaud, R.R. Gamache, A. Goldman, J.-M. Hartmann, K.W. Jucks, A.G. Maki, J.-Y. Mandin, S.T. Massie, J. Orphal, A. Perrin, C.P. Rinsland, M.A.H. Smith, J. Tennyson, R.N. Tolchenov, R.A. Toth, J. Vander Auwera, P. Varanasi, G. Wagner, J. Quantum Spectrosc. Radiat. Transf. **96**, 139 (2005)
40 A. Castrillo, G. Gagliardi, G. Casa, L. Gianfrani, Phys. Rev. A **67**, 062 503 (2003)
41 P. Werle, C. Dryoff, A. Zahn, P. Mazzinghi, F. D'Amato, Isotopes Environ. Health Stud. **41**, 323 (2005)
42 D.W. Schwenke, H. Partridge, J. Chem. Phys. **106**, 4618 (1997)
43 D.W. Schwenke, H. Partridge, J. Chem. Phys. **113**, 6592 (2000)